International Journal of Approximate Reasoning 55 (2014) 376–387

Contents lists available at ScienceDirect

International Journal of Approximate Reasoning

www.elsevier.com/locate/ijar

# Dealing with uncertainty and imprecision in image segmentation using belief function theory

Benoît Lelandais [a,*], Isabelle Gardin [b,a], Laurent Mouchard [a], Pierre Vera [b,a], Su Ruan [a]

[a] University of Rouen, LITIS EA 4108 – QuantIF, 22 bd Gambetta, 76183 Rouen, France
[b] Centre Henri-Becquerel, Department of Nuclear Medicine, 1 rue d'Amiens, 76038 Rouen, France

ARTICLE INFO

*Article history:*
Available online 16 October 2013

*Keywords:*
Belief function
Uncertainty
Imprecision
Information fusion
Image processing
Segmentation
Positron emission tomography

ABSTRACT

In imaging, physical phenomena and the acquisition system are responsible for noise and the partial volume effect, respectively, which affect the uncertainty and the imprecision. To address these different imperfections, we propose a method that is based on information fusion and that uses belief function theory for image segmentation in the presence of multiple image sources (multi-modal images). First, the method takes advantage of neighbourhood information from mono-modal images and information from an acquisition system to reduce uncertainty from noise and imprecision due to the partial volume effect. Then, it uses information that arises from each modality of the image to reduce the imprecision that is inherent in the nature of the images, to achieve a final segmentation. The results obtained on simulated images using various signal-to-noise ratios and medical images show its ability to segment correctly multi-modal images in the presence of noise and the partial volume effect.

© 2013 Elsevier Inc. All rights reserved.

## 1. Introduction

In imaging, information is imperfect. The imperfections can be separated into two main categories: uncertainty and imprecision. Both of these categories have a negative effect on image processing. They respectively correspond to a qualitative and quantitative defect in the knowledge. Noise, which originates from the inaccuracy of the image acquisition system with respect to reality, leads to the presence of uncertainty. Another problem in medical image processing is the presence of the partial volume effect. Originating from the limited spatial resolution of images and the sampling, the partial volume effect leads to the presence of imprecision. This effect results in a mixing of the intensities of neighbouring voxels, which is observed at the transition between regions. Moreover, in the medical image reconstruction process, a Gaussian filtering is applied, which increases the partial volume effect. The Gaussian filter is characterised by its Full Width at Half Maximum (FWHM), which is a measure that is proportional to the standard deviation of the Gaussian filter.

Belief Function Theory (BFT) [1–3] is especially well suited to representing information from partial and unreliable knowledge. BFT has the advantage of manipulating not only singletons but also disjunctions, which correspond, respectively, to simple and compound hypotheses. If manipulating singletons allows us to represent uncertainty as in probability theory, the manipulation of disjunctions allows us to represent imprecision. By assigning the Basic Belief Assignment (BBA) to singletons and disjunctions, both the uncertainty and the imprecision can be explicitly modelled. Using disjunctions, this approach makes it possible to account for the lack of knowledge. However, one of the difficulties resides in the modelling of

* Corresponding author.
*E-mail addresses:* benoit.lelandais@univ-rouen.fr (B. Lelandais), isabelle.gardin@chb.unicancer.fr (I. Gardin), laurent.mouchard@univ-rouen.fr (L. Mouchard), pierre.vera@chb.unicancer.fr (P. Vera), su.ruan@univ-rouen.fr (S. Ruan).

0888-613X/$ – see front matter © 2013 Elsevier Inc. All rights reserved.
http://dx.doi.org/10.1016/j.ijar.2013.10.006

the disjunctions. Although many methods for probability estimation on singletons are proposed in the literature, few methods use disjunctions. In [2,4,5], a modification of probabilistic models is proposed. This approach consists in transferring a part of a belief about disjunctions from a probabilistic distribution. Some methods are based on prior knowledge [6,7]. The disjunctions to be considered are determined in a supervised way. In [6], for example, trapezoidal functions are used for estimating the BBA on both singletons and disjunctions. Applied to multi-modal images, it is interesting to note that the image fusion, using Dempster's rule, allows them to model imprecision that corresponds to voxels that are subject to the partial volume effect. Indeed, their belief remains represented in disjunctions after the fusion. In [8], a modification of the k-nearest neighbour distance model is proposed. In this model, BBAs are estimated by combining, using Dempster's rule, the nearest neighbours, which are represented by two focal elements, the singleton that the neighbour belongs to and $\Omega$, which is weighted by a distance function. Data for which all of the neighbours are, respectively, close and distant will be represented on singletons and disjunctions. Indeed, uncertainty and imprecision are modelled according to the neighbourhood in the feature space. This model appears to be more efficient for segmenting medical images compared to a probabilistic model [9]. More recently, the Fuzzy C-Means (FCM [10]) distance-based algorithm has been generalised into the Evidential C-Means algorithm (ECM) [11], which allows to represent ambiguous information in the feature space on disjunctions in an unsupervised way. This algorithm has been modified, in [12], to add some constraints between clusters, and it has also been modified to account for proximity data [13], as initially proposed in [14]. Because these methods have not been introduced for modelling knowledge in image processing, the spatial relationships between voxels are not used.

Some methods that use belief function theory have been proposed specifically for image processing. In [15], the authors propose to use the histogram of the images for estimating the consonant mass distribution. The voxels for which a grey level has many occurrences, which are near a peak on the histogram, are mainly represented by the corresponding singleton. In contrast, the voxels for which the grey level has few occurrences, at the transitions between peaks, are mainly represented by disjunctions. The interest in this method arises from the use of the histogram to model the imprecision. However, this method does not consider the spatial relationship between voxels. In [16], the authors propose to use belief function theory in the Markov field context, which aims at benefiting from neighbourhood information for removing noise. The more general framework that is brought by the belief function allows us to account for the imprecision that is brought by the sources of the images. This Markov field extension is interesting for removing noise, but it has not been introduced for addressing the problem of the partial volume effect. A method for image fusion that presents occlusions is proposed in [17]. This method consists in using the neighbourhood information for addressing imperfections. First, imprecision due to occlusions is modelled with disjunctions on each image. Then, the fusion of each voxel with a mass function, which represents the neighbourhood and uses a normalised sum operator, is conducted to model the uncertainty. The authors make the assumption that this compromise rule is well adapted at first, before combining multiple images. Finally, an iterative regularisation process, which is similar to a Markov field, is performed to improve the decision. Despite uncertainty due to noise, the imprecision due to occlusions is managed, and the imprecision due to the partial volume effect is not considered. In [18], an approach that performs a conjunctive combination of neighbouring voxels has been proposed. On the one hand, this approach allows for each voxel to reduce the uncertainty due to noise and imprecision due to the partial volume effect by transferring part of the belief on singletons according to its neighbourhood. On the other hand, it allows us to consider very ambiguous voxels that correspond to transitions between regions in which the partial volume effect occurs on the empty set. Some authors have investigated this method for the segmentation of medical images [9,19,20]. In [20], the approach is especially interesting because the fusion of neighbourhood information is integrated into the ECM algorithm [11]. This process updates cluster centres from data whose noise and partial volume effect are reduced. Currently, this approach has not been introduced for modelling the imperfections on disjunctions. In [21], the author proposes to use fuzzy morphological operators for modelling imperfection from initial BBAs. This goal is achieved by transferring, for each voxel, a part of the belief on disjunctions according to its neighbourhood either in feature space or in the image. This method allows us to consider both the uncertainty and the imprecision in the disjunctions. By combining multiple complementary images to model imperfections, uncertainty due to noise can be reduced, whereas imprecision due to the partial volume effect remains represented in the disjunctions. Because BFT can model differentially these two imperfections and because neighbourhood information is sufficient for reducing the uncertainty, it could be interesting to reduce the uncertainty and model the imprecision on mono-modal images and then use multiple pieces of information to remove the imprecision.

Our aim is two-fold: first, to reduce the uncertainty due to noise, and then, to reduce the imprecision due to the partial volume effect, which corresponds to the lack of knowledge at the transitions between areas. For this purpose, BFT is used. We call our method Evidential Voxel-based Estimation of Imperfect Information (EVEII). First, our method operates a disjunctive combination followed by a conjunctive combination of neighbouring information on mono-modal images. The disjunctive combination allows us to transfer both uncertain and imprecise information on disjunctions. Then, the conjunctive combination is applied to reduce the uncertainty due to noise while maintaining a representation of imprecise information at the boundaries between the areas on the disjunctions. To remove the imprecise information that is considered on the disjunctions, fusion with an a priori contextual knowledge that is represented by a simple mass function related to the acquisition system is proposed. Finally, a multi-modal image fusion is proposed. We benefit from the complementarity of images to reduce the imprecisions that are inherent in the nature of these images.

The method is applied to the fusion of multi-tracer PET (Positron Emission Tomography) medical images of the same patient. Three radiotracers are used to provide information on tumour glucose metabolism, cell proliferation, and hypoxia

(inadequate supply of oxygen). These images are of major interest for the treatment of lung cancer by radiotherapy, but relevant image processing is required to address both the important noise and the partial volume effect.

First, we present BFT. Then, we describe our method, which is based on fusion in mono-modal images followed by a multi-modal fusion of information. Then, the validation of the method is performed on simulated data. Finally, the method is applied to multi-tracer PET images to segment tumours.

## 2. Segmentation method based on information fusion

In this section, first, we present our EVEII method for reducing uncertainty in the case of one image (a mono-modal image). This case consists in estimating Basic Belief Assignments (BBAs) of voxels by using combination operators of BFT. This approach requires the definition of the frame of discernment, the information sources, and the neighbourhood. Second, we present how to reduce both the uncertainty and the imprecision by using multi-modal information. Uncertainty is reduced by using the fusion of each voxel with its neighbours, and imprecision is then reduced by using the fusion of each voxel with the prior knowledge obtained from the acquisition system.

### 2.1. EVEII: Evidential Voxel-based Estimation of Imperfect Information

#### 2.1.1. Context

Let $\Omega = \{\omega_1, \omega_2, \ldots, \omega_C\}$ be a finite set of classes, called the *frame of discernment*. Partial knowledge, which flows out from the information sources, is accounted for when using BFT by assigning BBAs or masses, $m$, over different subsets of the frame of discernment. In image processing, each voxel $V_i$ constitutes a source of information that is associated with a specific BBA from $2^\Omega = \{\emptyset, \{\omega_1\}, \{\omega_2\}, \ldots, \{\omega_C\}, \{\omega_1, \omega_2\}, \ldots, \Omega\}$ to $[0, 1]$. Because our EVEII method has been designed to account for the uncertainty and imprecision in a mono-modal image but not to detect outliers, the closed-world assumption is considered.

To account for the information that is contained in the environment of $V_i$, the neighbouring voxels are considered. The neighbourhood is defined as follows: let $\Phi(V_i)$ be a set of $K$ voxels $V_k$ (with $k \in \{1, \ldots, K\}$) that surround a voxel $V_i$ and include $V_i$. Because of the different distances that separate $V_k$ and $V_i$, for each voxel in $\Phi(V_i)$, we propose to associate to $V_k$ a coefficient $\alpha_k$ that depends on the distance that separates it from $V_i$. This value is computed by:

$$\alpha_k = \exp\left(-(V_k - V_i)^2/\sigma^2\right) \tag{1}$$

with $\sigma = \text{FWHM}/(2\sqrt{2\log 2})$, where FWHM is the Full Width at Half Maximum, which corresponds to the spatial resolution of the image. For example, let FWHM $= 5$ mm be the measure of the spatial resolution in an image. Let $V_i$ be a voxel, and let $V_k$ be a neighbour whose physical distance to $V_i$ is 2.5 mm. Thus, a coefficient $\alpha_k = 0.5$ that is computed using Eq. (1) is associated with $V_k$ and corresponds to the contribution that $V_k$ has toward $V_i$. The farther away from $V_i$ that the voxel $V_k$ is, the lower the value of $\alpha_k$.

#### 2.1.2. BBA estimation considering both the uncertainty and the imprecision on mono-modal images

We propose a BBA estimation that considers both the uncertainty and the imprecision. This method can use either an initial BBA estimation, which can be obtained from a priori knowledge given by an expert, or by using a clustering algorithm such as Fuzzy C-Means (FCM) [10].

*With initial BBAs (EVEII$_1$)* If an initial BBA estimation is already available, then we propose to apply the following operation to transfer ambiguous information on compound hypotheses. Here, the well-known FCM algorithm is used, but other distributions could even be used. This approach allows us to associate with each voxel a fuzzy membership degree toward each class in an unsupervised way. In our case, the algorithm is applied on a feature space that corresponds to grey levels for initialising BBA over $m_{V_k}(\{\omega_c\})$, with $\omega_c \in \Omega$.

First, the influence of a voxel $V_k$ from $\Phi(V_i)$ is weighted by the coefficient $\alpha_k$. The BBA on $A \neq \emptyset$ and on $\emptyset$ can be calculated by using the expressions:

$$\begin{aligned} m'_{V_k}(A) &= \alpha_k m_{V_k}(A), \quad \forall A \neq \emptyset \\ m'_{V_k}(\emptyset) &= 1 - \alpha_k + \alpha_k m_{V_k}(\emptyset) \end{aligned} \tag{2}$$

The transfer to the empty set is interpreted as a non-commitment toward all of the other hypotheses, allowing us to reduce the influence of $m_{V_k}(A)$ proportionally to $\alpha_k$ before applying a disjunctive combination. At this stage, the closed-world assumption is not verified because non-null masses are affected to the empty set according to $\alpha_k$. However, this statement is only true for the neighbours $V_k$ and not for $V_i$. Because of the next step, the masses on the empty set become null, and the closed-world assumption can be made on our global process.

After this step, to transfer uncertain and imprecise data to disjunctions, the disjunctive combination of each voxel with each of its neighbours is performed [5]. The combination of a voxel $V_i$ with one of its neighbours $V_k$ is given by:

**Table 1**
Illustration of the combination of a voxel $V_i$ with one of its neighbours $V_k$. Here, $m$ is the mass distribution that is obtained by using the FCM algorithm with two classes; $m'$ is the mass distribution from applying our weight function; and $\mathcal{M}$ is a result of the combination of $m'_{V_i}$ and $m'_{V_k}$ using the disjunctive rule.

| $A$ | $m_{V_i}(A)$ | $m_{V_k}(A)$ | $m'_{V_i}(A)$ | $m'_{V_k}(A)$ | $\mathcal{M}_{V_i}(A)$ |
|---|---|---|---|---|---|
| $\emptyset$ | 0 | 0 | 0 | $(1-\alpha_k)$ | 0 |
| $\{\omega_1\}$ | $x$ | $y$ | $x$ | $\alpha_k \cdot y$ | $x(1-\alpha_k(1-y))$ |
| $\{\omega_2\}$ | $1-x$ | $1-y$ | $1-x$ | $\alpha_k(1-y)$ | $(1-x)(1-\alpha_k y)$ |
| $\{\omega_1,\omega_2\}$ | 0 | 0 | 0 | 0 | $\alpha_k(x+y-2xy)$ |

$$\mathcal{M}_{V_i}(A) = \sum_{B\cup C=A} m'_{V_i}(B)\cdot m'_{V_k}(C) \tag{3}$$

and can be generalised to the set of voxels in the neighbourhood because the operator is commutative and associative. This combination allows us to assign non-zero masses to disjunctions. The higher they are, the more different is the information that is carried by the neighbouring voxels. This relationship is especially true for voxels for which the partial volume effect is present and for voxels that are located in a very noisy environment. This operator is usually used when at least one source is reliable. In the context of image processing, it is reasonable to assume that at least one of the voxels in the neighbourhood gives reliable information. Although a voxel $V_i$ is unreliable, the disjunctive combination of the neighbouring voxels leads to represent it on a compound hypothesis, which increases the ignorance. Thus, after the disjunctive combination, the process acts as a discounting for unreliable voxels.

Let $V_i$ be a voxel, and let $V_k$ be a neighbour; these two voxels are associated with the coefficients $\alpha_i = 1$ and $\alpha_k$, respectively. The BBAs associated with $V_i$ and $V_k$, which are given by the FCM algorithm, are $m_{V_i}(\{\omega_1\}) = x$, $m_{V_i}(\{\omega_2\}) = (1-x)$, $m_{V_k}(\{\omega_1\}) = y$ and $m_{V_k}(\{\omega_2\}) = (1-y)$, as presented in Table 1. The table illustrates their weighting and their combination using Eqs. (2) and (3), respectively. As we can see, the weight function allows us to transfer a part of the belief on the empty set. Because the mass on the empty set for the voxel $V_i$ is null, the closed-world assumption after the combination remains verified. On $\{\omega_1\}$, the result of the combination is proportional to $x$ but not $y$ because of our weight function, which means that the influence of $V_k$ has been reduced according to $\alpha_k$. The same behaviour is observed concerning $\{\omega_2\}$. Finally, the mass on $\{\omega_1,\omega_2\}$ after the combination is proportional to $(x+y-2xy)$, which takes high values when $V_i$ and $V_k$ are discordant. When $V_i$ and $V_k$ are consistent, it takes medium values if the values of $x$ and $y$ are close to 0.5 and low values otherwise. Moreover, it is weighted by $\alpha_k$, which takes a low value if $V_k$ is physically distant from $V_i$. Thus, the farther away from $V_i$ the voxel $V_k$ is, the lower its contribution to the computation.

*Without initial BBA (EVEII$_2$)* As presented above, the disjunctive combination of neighbouring voxels allows us to transfer uncertain and imprecise information on disjunctions from initial BBAs that are computed using FCM. To estimate the BBAs more precisely, we propose to integrate this combination inside the FCM algorithm [22]. First, the masses are estimated by using the following equation:

$$m_{V_i}(\{\omega_c\}) = \frac{1}{\sum_{t=1}^{C}\left(\frac{d_{ic}}{d_{it}}\right)^{\frac{2}{\gamma-1}}} \tag{4}$$

where $d_{i,c}$ is the Euclidean distance between the grey value of the voxel $V_i$ and the centre of class $c$, and $\gamma$ is the parameter that controls the fuzziness of the partition ($\gamma = 2$ by default). Our contribution resides in the integration of neighbouring information by computing $\mathcal{M}$ using Eqs. (2) and (3). As explained in the previous paragraph, voxels that are subject to noise and the partial volume effect are represented on disjunctions, whereas voxels that are not subject to these imperfections are represented on singletons. Then, cluster centres are updated at each iteration with the following equation:

$$\mathbf{v}_c = \frac{\sum_{i=1}^{N}(\mathcal{M}_{V_i}(\{\omega_c\}))^{\gamma}\cdot I_{V_i}}{\sum_{i=1}^{N}(\mathcal{M}_{V_i}(\{\omega_c\}))^{\gamma}}, \quad \forall c = \{1,\ldots,C\} \tag{5}$$

where $\mathbf{v}_c$ is the centre of the $c$ class and $I_{V_i}$ is the intensity of the voxel $V_i$. Because the feature space is one-dimensional (grey levels), the centre $\mathbf{v}_c$ is defined in $\mathbb{R}$. The difference from the FCM algorithm is that it is not membership degrees that are used but instead the masses according to the singletons obtained after the neighbourhood combination. As a result, the voxels that present ambiguity are not considered in the cluster centre updating. Indeed, their masses are spread over disjunctions, and only the masses over singletons are considered in the updating.

Thus, the FCM algorithm works only with precise and certain data, which leads to a better BBA estimation. Similar approaches are proposed in [11,20]. In contrast to [11], our method uses a spatial relationship to transfer the BBAs over compound hypotheses. In contrast to [20], we use the disjunctive combination, which does not reduce the noise during the iteration process rather than the conjunctive combination. In addition, our method does not account for the noisy data during the updating process to compute the cluster centres.

*2.1.3. Conjunctive combination of neighbouring voxels*

With BTF, disjunctions are mostly used for modelling imprecision due to a lack of knowledge. Our method as previously presented allows us to represent on disjunctions the imprecise information as desired and also the uncertain information. To address this phenomenon, the opposite operation is proposed, namely the conjunctive combination of neighbouring voxels. This approach aims at reducing both the uncertainty and the imprecision mainly by transferring the information toward singletons, in contrast to the previous stage. However, because of a lack of knowledge at the transition between the regions, imprecisions are not completely reduced. Thus, this process can be used for reducing uncertainty but not imprecision.

First, discounting is performed according to the same coefficient $\alpha_k$ as before, by transferring a part of a belief onto the set $\Omega$:

$$\begin{aligned} \mathcal{M}''_{V_k}(A) &= \alpha_k \mathcal{M}_{V_k}(A), \quad \forall A \neq \Omega \\ \mathcal{M}''_{V_k}(\Omega) &= 1 - \alpha_k + \alpha_k \mathcal{M}_{V_k}(\Omega) \end{aligned} \tag{6}$$

The discount process allows us to reduce the influence of voxels that are located physically far away from $V_i$ before the conjunctive combination. Because all of the voxels whose neighbourhood is discordant are represented with disjunctions after the disjunctive combination, very low masses are assigned to the empty set by using the conjunctive rule. However, to respect the closed-world assumption, we propose to use Dempster's rule [1]. The combination of a voxel $V_i$ with one of its neighbours $V_k$ is given by:

$$M_{V_i}(A) = \frac{1}{1-\kappa} \sum_{B \cap X = A} \mathcal{M}''_{V_i}(B) \cdot \mathcal{M}''_{V_k}(X) \tag{7}$$

where $\kappa$ is the mass on the empty set in the open-world assumption. Dempster's rule consists in normalising the conjunctive rule by the conflict between sources. This approach can be generalised to the set of voxels in the neighbourhood because the operator is commutative and associative. Because all voxel-sources can be considered to be reliable after the above processing due to the disjunctive combination, the fusion operation is performed properly. This step allows us to remove uncertainty due to noise, by transferring their belief onto the singletons, while the imprecision due to the partial volume effect, whose neighbourhood information does not allow us to reduce it, remains represented on the disjunctions.

Note that by using the FCM algorithm, the membership degrees do not decrease with respect to the distance to the cluster centre due to normalisation. Thus, the voxels that are subject to this effect are considered to be uncertain in our BBA estimation process. Because of this conjunctive combination of neighbouring information, this problem is inhibited.

*2.2. Fusion for reducing the imprecision using an external knowledge*

Using mono-modal images, our EVEII method benefits from neighbourhood information to model imprecision on disjunctions and to reduce the uncertainty. To reduce the imprecision, multi-modal information is necessary. Using multiple sources, the reduction can be achieved by applying conjunctive or Dempster's combination rules. We propose to use a priori contextual knowledge, which is related to the spatial resolution of the acquisition system, to reduce imprecisions for our application to PET images (Section 4). The imprecision, due to the partial volume effect, corresponds to a contamination of neighbouring structures and leads to an under-estimation of the tumour volume. The lower the contrast and the size of the tumour are, the higher the imprecision is. We propose to reduce the imprecision, when represented on disjunctions, by transferring a part of the belief to the subset that corresponds to the tumour, according to a function called $\beta$. In our segmentation problem, $\beta$ is a function that depends on both the volume of the tumour and the contrast between the tumour and the background that is measured on the images after applying EVEII. The function $\beta$ is built from a set of eight contrast PET phantom images that contain eight spheres, by measuring the part of the belief that must be transferred to the subset that corresponds to the tumour for each sphere and each contrast. In PET images, the subset that corresponds to the tumour is characterised by high grey values. Because the same acquisition system is used in both cases, PET phantom images and patient images have the same spatial resolution. After having applied EVEII and measured $\beta$ for the patient images, we propose the following simple mass function, which has two focal elements for representing the a priori contextual knowledge:

$$\begin{aligned} m_\beta(A) &= \beta \\ m_\beta(\Omega) &= 1 - \beta \end{aligned} \tag{8}$$

where $A$ is the subset to reinforce. Then, the combination of each voxel-source with this BBA is applied using Dempster's rule:

$$\mathcal{M}_{V_i}(A) = \frac{1}{1-\kappa'} \sum_{B \cap X = A} M_{V_i}(B) \cdot m_\beta(X) \tag{9}$$

where $\kappa'$ is the mass on the empty set in the open-world assumption. This process allows us to transfer a part of the belief to the subset $A$ that corresponds to the tumour in PET and, thus, to reduce the imprecision.

The reduction in the imprecision is applied over the entire image, but it has an influence only where the partial volume effect occurs. Indeed, ignorance is considered only at the transition between regions after using EVEII. This approach involves a contextual reinforcing and corresponds to the inverse process to contextual discounting, which is presented in [23].

## 3. Validation

### 3.1. Simulated images

The efficiency of our method is evaluated and compared with the method proposed in [10,21,11,20] on two simulated images (size $100 \times 100$ pixels). The two simulated images have a square surrounded by background (images with two classes, $\omega_1$ and $\omega_2$). The difference between the two images concerns the size of the square. The first image contains $50 \times 50$ pixels, and the second image contains $10 \times 10$. To simulate the partial volume effect, the images are blurred with a Gaussian filter whose FWHM equals 5 pixel-widths. Then, noise is added by using a Gaussian filter whose Signal-to-Noise Ratio (SNR) equals 5 too. The two images are presented in Figs. 1(a) and 2(a). Note that the second square does not look like a square due to blurring.

### 3.2. Evaluation

#### 3.2.1. Imperfection modelling

Our proposed method, EVEII, is applied on both simulated images. First, it is applied from an initial BBA estimation given by the FCM algorithm ($\text{EVEII}_1$). Second, it is applied without an initial BBA estimation ($\text{EVEII}_2$). Two results are given that are compared with five methods: the FCM algorithm [10], the method using mathematical morphology for transferring BBAs on disjunctions [21] (MORPHO), the ECM algorithm [11], the ECM algorithm followed by a conjunctive combination of neighbourhood information as presented in Section 2.1.3 ($\text{ECM}_c$), and the MECM algorithm [20], which applies a conjunctive combination of neighbourhood information inside the ECM algorithm. The parameter $m$ is set to 2 for the FCM and EVEII algorithms. We set $\alpha = 1$, $\beta = 2$ and $\delta = 1$ for the ECM and MECM algorithms. Using the default value $\alpha = 2$, imprecision is not modelled in a satisfying way, which leads to problems for $\text{ECM}_c$ and for the MECM methods that attempt to slightly reduce the imprecision by using the conjunctive rule of combination. Concerning $\beta$, we did not note a positive influence by modifying the default value $\beta = 2$. Note that, when $\delta = 1$, there are no outliers. The minimum *t-norm* operator is used for fuzzy erosion in the MORPHO method and has been applied to spatial domains. For all of the methods that use neighbourhood information, the same structuring element as the element that was applied for blurring images is used (a Gaussian filter with FWHM = 5 pixel-width).

The results presented in Fig. 1 show the performance of each method from using the first simulated image. The result of the FCM algorithm is presented in Fig. 1(b). Because we used this result for assigning BBAs over singletons, the disjunctions for modelling imprecision are not considered. Thus, this approach yields poor imperfection modelling. Using the same initial BBA estimation that is provided by FCM, we can compare our $\text{EVEII}_1$ method (with initial BBA; Figs. 1(c) and (d)) to the MORPHO method introduced in [21] (Fig. 1(f)). Using $\text{EVEII}_{1d}$, at the end of the disjunctive combination of each pixel with its neighbourhood, the belief masses are spread over the hypotheses $\{\omega_1\}$, $\{\omega_2\}$ and $\{\omega_1, \omega_2\}$ (Fig. 1(c)). The belief of each pixel for which the information is ambiguous is mainly represented on the hypothesis $\{\omega_1, \omega_2\}$. Then, using the conjunctive combination of each pixel with its neighbourhood, the result of $\text{EVEII}_1$ is obtained and is presented in (Fig. 1(d)). Inside the areas, the method provides high beliefs in favour of $\{\omega_1\}$ and $\{\omega_2\}$. The uncertainties due to noise are therefore reduced. Within the transitions between areas, the belief is mainly represented on the hypothesis $\{\omega_1, \omega_2\}$, which highlights the imprecision due to the partial volume effect. In comparison, MORPHO considers both noisy and fuzzy information as imprecision. Indeed, both the pixels inside the regions and the pixels at the transitions between the regions are represented on the disjunction $\{\omega_1, \omega_2\}$. This representation arises because MORPHO benefits from intensity variation in the neighbourhood of each voxel when transferring information toward disjunctions. Thus, the result is closed to those who use the disjunction combination of neighbourhood information (see Fig. 1(c)). In $\text{EVEII}_1$, the conjunctive combination of neighbouring pixels allows us to reduce noise and consider only fuzzy information on disjunctions. Our second $\text{EVEII}_2$ method (without an initial BBA) is also compared. Using the disjunctive combination inside the FCM algorithm offers similar results compared with using separately the same two operations on this simulated image. Comparing EVEII to ECM (Figs. 1(g) and (e)), we see that ECM considers both uncertain and imprecise information on the disjunction, whereas EVEII considers these two imperfections in a different manner because of the spatial relationships between the pixels. Then, the results are obtained by applying a conjunctive combination of the neighbouring information and are given in Fig. 1(h). These results are similar to the result given in Fig. 1(i), which applies the combination inside the ECM algorithm. This combination inside ECM allows reducing uncertainty due to noise and also imprecision due to the partial volume effect. Using this scheme, cluster centre updating is performed by using masses for which a reduction in uncertainty is performed, which induces biases. Moreover, recall that the partial volume effect is mainly present at the transition between regions and corresponds to a lack of knowledge that should be represented with disjunctions, from our perspective. Remark that the structuring element, which is the same as the element that is used for blurring simulated images, is perhaps too large at this time, when using only ECM for estimating the imprecision.

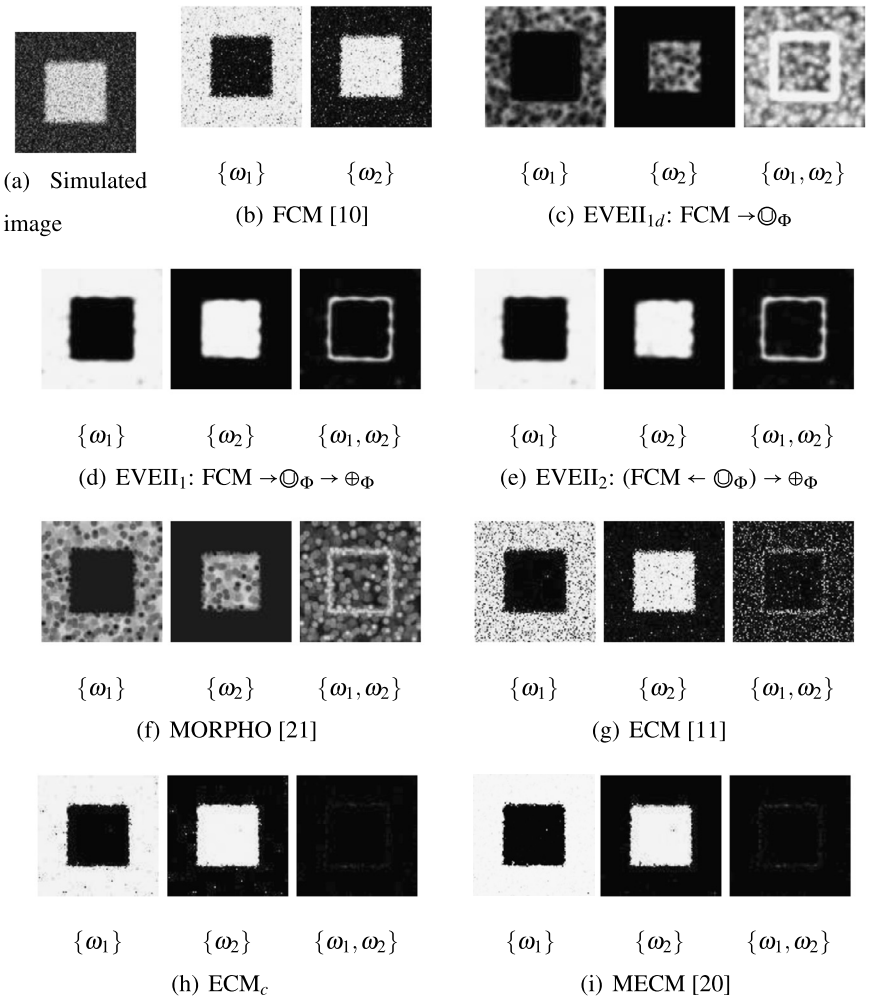


**Fig. 1.** Imperfection modelling of the simulated image presenting a large blurred and noisy square (a) using our EVEII method and five other methods for comparison. (b) is the result using FCM. (c), (d) and (e) are the results using our EVEII method. (c) is obtained after applying the disjunctive combination of neighbouring information after FCM. (d) is the result from applying the conjunctive combination of the neighbouring information. (e) is the result of using first the disjunctive combination inside the FCM algorithm and then the conjunctive combination. (f), (g) and (i) are the results of using the methods proposed in [21], [11] and [20], respectively. (h) corresponds to the ECM algorithm followed by a conjunctive combination of neighbourhood information.

We also propose to compare the methods using the second simulated image given in Fig. 2(a), whose square is smaller than the square studied in the previous simulated image. The important point to note is that FCM and ECM, whose results are given in Figs. 2(b) and (g), provide a poor BBA estimation; BBAs for noisy data in the background are represented on the hypothesis $\{\omega_2\}$, while $\{\omega_1\}$ should be used. The reason is that the amount of noisy data in the background is too large compared with the amount of data in the square, which results in a biased estimation of the cluster centres. The way for providing good cluster centre estimation is to benefit from the neighbourhood contribution inside the clustering iteration process. The best results are effectively obtained with MECM and our EVEII$_2$ method, which are given in Figs. 2(i) and (e). As previously noted, the difference between these two methods is that one reduces both the uncertainty and the imprecision before updating the cluster centres (MECM), and the other does not consider both the uncertainty and the imprecision for cluster centre updating and reduces the uncertainty and some of the imprecision after the iterative process only. Moreover, for pixels that are subject to important noise, because of the disjunctive combination of neighbouring pixels for transferring at the first stage noisy information over disjunctions, noise is better reduced using EVEII$_2$ than MECM.

### *3.2.2. Performance in segmentation*

The efficiency of our method is also evaluated and compared with the method proposed in [10,21,11,20] on the first simulated images according to a Gaussian blurring whose FWHM ranges from 8.5 to 4 (in steps of $-0.2$) and a Gaussian noise whose SNR ranges from 1.5 to 6 (in steps of 0.2). Five simulated images are presented at the bottom of Fig. 3. Dice's coefficient is a similarity measure that is used for making a comparison of two results. Let $X$ and $Y$ be the true area and

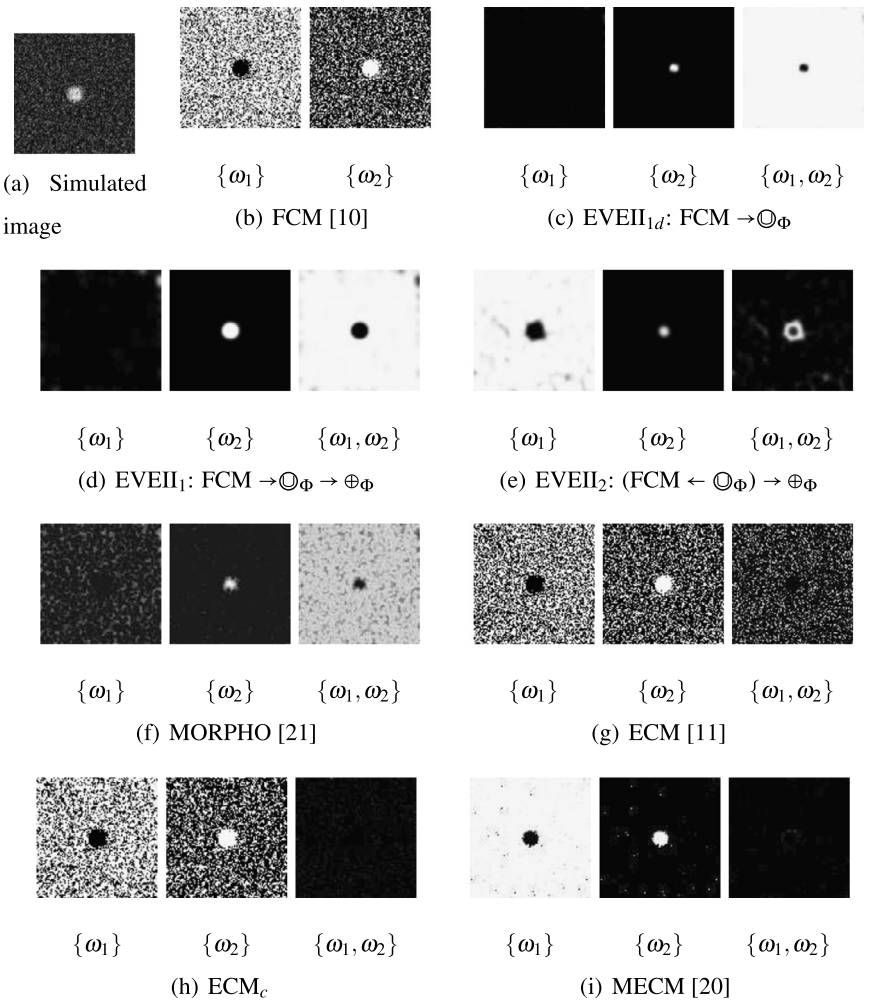


**Fig. 2.** Imperfection modelling of the simulated image, which presents a slightly blurred and noisy square (a), when using our EVEII method and five other methods for comparison. (b) is the result from using FCM. (c), (d) and (e) are the results from using our EVEII method. (c) is obtained after applying the disjunctive combination of neighbouring information after FCM. (d) is the result from then applying the conjunctive combination of the neighbouring information. (e) is the result from first using the disjunctive combination inside the FCM algorithm and then using the conjunctive combination. (f), (g) and (i) are the results from using the methods proposed in [21], [11] and [20], respectively. (h) corresponds to the ECM algorithm followed by a conjunctive combination of neighbourhood information.

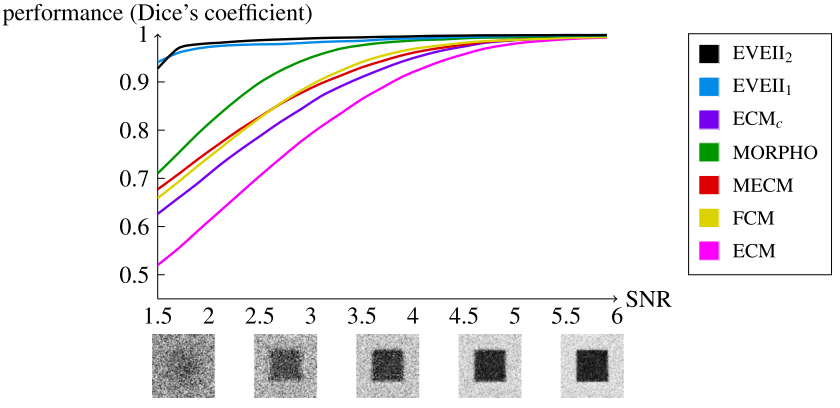


**Fig. 3.** Presentation of Dice's coefficient according to different SNRs on simulated images using the seven methods presented on the right. From the bottom to the top: the ECM algorithm [11], the ECM followed by the conjunctive combination of neighbourhood information (ECM$_c$), the MECM algorithm [20], the FCM algorithm [10], the method proposed in [21], and our EVEII methods. This graph is better presented in colour (see the web version of the article).

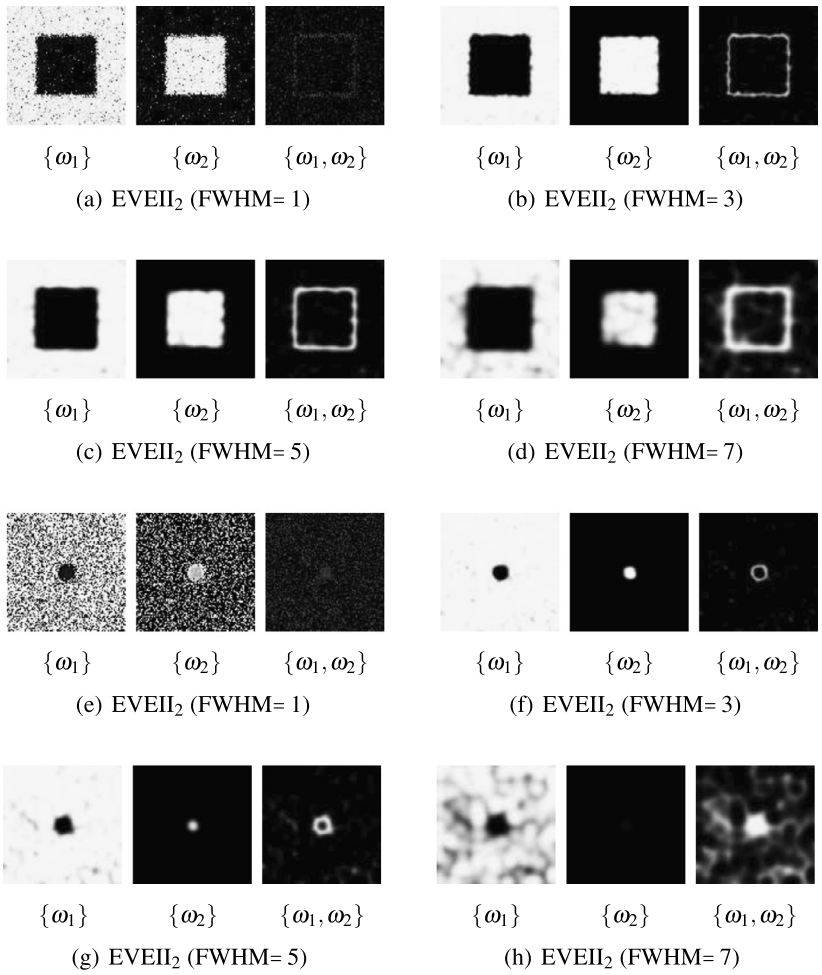


**Fig. 4.** Illustration of the neighbourhood influence using our $EVEII_2$ method and four Gaussian structuring elements that vary according to their FWHM. The results are given in (a), (b), (c) and (d) for the first simulated image (see Fig. 1(a)), and in (e), (f), (g) and (h) for the second simulated image (see Fig. 2(a)). For each result, FWHM equals 1, 3, 5 and 7 pixel-width.

the segmented area obtained by using one of these methods. Dice's coefficient gives a similarity measure between the two areas; this measure is given by:

$$s = \frac{2|X \cap Y|}{|X| + |Y|} \tag{10}$$

To measure Dice's coefficients for each SNR, the methods are applied here on two images that have the same SNR, and the results are then fused using Dempster's rule to reduce the uncertainty. Because some of the methods that were compared, such as MORPHO and ECM, have not been introduced for reducing the uncertainty, the use of two images and their fusion is necessary to perform a relevant comparison. Moreover, because of noisy data, and in order to ensure a good statistical measurement, Dice's coefficient is computed using 20 different replicas per simulated image. The Dice coefficients that correspond to average values ($N = 20$) are given in Fig. 3.

As can be seen in Fig. 3, FCM gives better results than ECM. This finding is because ECM is more sensitive than FCM to the unequal data distribution between the classes. Indeed, the number of pixels is higher in the background than in the square, and imprecise data are principally found in the background when using ECM (see Fig. 1(g)). In $ECM_c$ and MECM, the use of neighbourhood information allows to improve Dice's coefficients compared to the use of ECM only. The improvement is also found using the neighbourhood contribution with the FCM algorithm, as in MORPHO and $EVEII_1$. Better Dice coefficients are obtained with our $EVEII_1$ method. Moreover, when a disjunctive rule is integrated into FCM, the performances are slightly improved ($EVEII_2$ vs. $EVEII_1$). This improvement is due to the robustness of $EVEII_2$ with respect to the unequal data distribution between the classes.

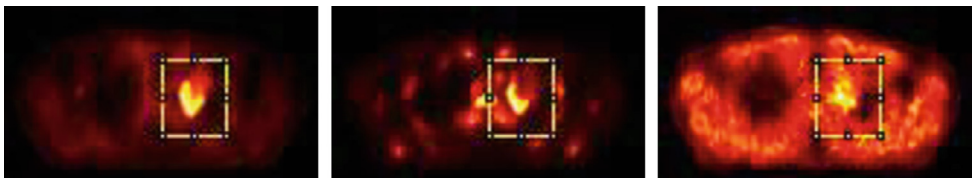

(a) FDG (b) FLT (c) FMISO

**Fig. 5.** Transverse slices for one patient with lung cancer. (a) Glucose metabolism PET image, (b) cell proliferation PET image, (c) hypoxia PET image. The area of interest (tumour lesion) is located in the rectangle.

**Table 2**
Hypotheses that were considered for the PET images, to fuse them coherently.

| Image | Low uptake | High uptake | $\Omega$ |
|---|---|---|---|
| FDG | $\{N\}$ | $\{M, P, H, F\}$ | $\{N, M, P, H, F\}$ |
| FLT | $\{N, M, H\}$ | $\{P, F\}$ | $\{N, M, P, H, F\}$ |
| FMISO | $\{N, M, P\}$ | $\{H, F\}$ | $\{N, M, P, H, F\}$ |

*3.2.3. Neighbourhood influence*

To evaluate the neighbourhood influence, our EVEII$_2$ method is applied on two simulated images for which the neighbourhoods have different sizes. Four Gaussian structuring elements are considered. They have an FWHM of 1, 3, 5 and 7 pixel-width, respectively. The results are presented in Fig. 4. When FWHM $= 1$, as we can see in Figs. 4(a) and (e), the noise is not reduced, which indicates that the neighbourhood size must be relatively large to account for the spatial contribution and, thus, to reduce the noise. As can be seen in Figs. 4(b), (c), (d), (f), (g) and (h), the uncertainty due to noise is reduced, while imprecision due to a partial volume effect is represented in the disjunctions. The higher the FWHM, the higher the number of pixels that are represented in the disjunction. For our simulated image, with FWHM $= 7$ pixel-width, the imprecision that is modelled appears to be too large, especially in Fig. 4(h). Indeed, the size of the structuring element corresponds to a compromise between the amount of noise and the amount of partial volume effect. A good compromise is obtained using FWHM $= 3$ or 5 pixel-width for our image. The trade-off depends on the spatial resolution of the image acquisition system and the sampling that is chosen. These sizes can be chosen empirically in the applications.

## 4. Application to multi-modal PET images for functional tumour localisation

The proposed method is applied to the fusion of multi-tracer PET functional medical images (Fig. 5) to localise a tumour. These images are obtained after the injection of a tracer that is specific to a studied function. Using the FDG, FLT and FMISO tracers, three types of PET images are obtained for a patient. These tracers highlight the glucose metabolism, cell proliferation and hypoxia (an inadequate supply of oxygen). The FDG provides a good definition of the tumour target volume for radiation therapy, especially ganglionic [24]. The FLT has a better tumour specificity than FDG [25] and lets us envisage increasing the frequency of radiation therapy sessions on hyper-proliferative lesions. Finally, FMISO defines hypoxic tumours for which an irradiation dose escalation can be envisaged to improve the treatment [26].

The three PET images allow the distinction of areas that can be represented by five singletons, namely healthy tissue $\{N\}$ ($N$ormal), those with an important glucose $M$etabolism $\{M\}$, an important cell $P$roliferation $\{P\}$, a significant $H$ypoxia $\{H\}$, and tissues with a $F$ull uptake $\{F\}$, where tissues need an increase in both the radiation therapy frequency and the dose. For each image, the proposed EVEII$_2$ method (without an initial BBA estimation) has been applied to obtain BBAs for the three hypotheses, which correspond to low uptake, high uptake and their union, as presented in Table 2.

On the PET images, the partial volume effect depends on both the size of the tumour area (the tumour presents a high uptake) and the contrast between the tumour and the background (the background presents a low uptake). Thus, it becomes important to reinforce the BBA of high-uptake areas according to its contrast and its volume. We chose to apply the reinforcement presented in Section 2.2 with knowledge that depends on contrast and volume. This step allows us to improve the modelling by reducing the imprecision on each mono-modal PET images.

The results obtained from multi-modal PET images (Fig. 5) are presented in Fig. 6. Figs. 6(a) to (f) present BBAs that correspond to high-uptake tissues and imprecise information after applying our fuzzy clustering method on each image followed by the conjunctive combination of neighbouring voxels. On the one hand, we observe that noisy information is removed from areas that correspond to high-uptake tissues. On the other hand, we can see that areas that correspond to the partial volume effect and medium uptake are assigned mainly to the compound hypotheses. Figs. 6(g) to (k) present the fusion result by first using the reinforcing step and then using the conjunctive combination of the multi-tracer PET images. Because low masses are assigned to disjunctions, the imprecision is reduced. The conflict is presented in Fig. 6(g) and corresponds to a high uptake in FLT or FMISO and a low uptake in FDG. Here, in the chosen example, the conflict that appears on the left of the image (Fig. 6(g)) corresponds to the normal physiological behaviour of bone marrow cells, with an important cell proliferation (high FLT uptake). Figs. 6(h) to (k) are the plausibilities that correspond to our hypotheses of

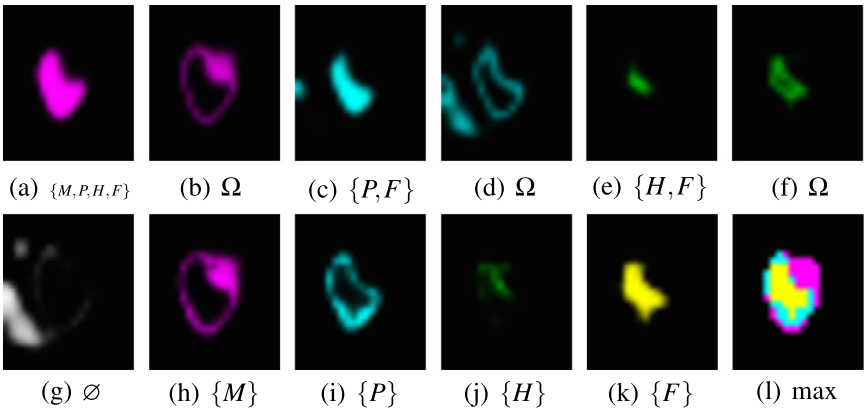


**Fig. 6.** Images that show the results of our multi-modal PET image fusion method. Each image corresponds to a specific set, and the higher the intensity of a voxel is, the higher the belief mass or the plausibility. (a) to (f) show the BBAs that are assigned to each voxel after the estimation step. (g) to (l) are the results from applying Dempster's rule of combination. (g) corresponds to the areas of conflict. (h) to (k) represent the plausibility that corresponds to our hypotheses of interest. Finally, (l) is the segmented image from using the maximum of the plausibility.

interest: $\{M\}$, $\{P\}$, $\{H\}$ and $\{F\}$. Finally, Fig. 6(l) corresponds to the segmented tumour that results from using the maximum of the plausibility. This image is of great interest for the radiation oncologist because it is used to adapt the dose deliverance according to several physiological behaviours of tumour tissues.

## 5. Conclusions

Currently, in medical images, very few authors consider both spatial uncertainty and imprecision when modelling the information with the BFT [21]. We propose an EVEII method that performs a fusion of neighbouring information by a disjunctive combination followed by a conjunctive combination. This method allows us to address both types of imperfection. In addition, we suggest integrating the disjunctive combination into FCM to compute the cluster centres by using only certain and precise information. Then, we propose to draw from prior knowledge to reduce imprecisions that are due to the partial volume effect. Finally, a multi-tracer (multi-modal) image fusion is proposed. We draw from the complementarity of the images to reduce the imprecisions that are inherent to the nature of the images.

As shown from the results on simulated and medical images, the main interest in our method arises because the uncertainties due to noise are largely removed, and the imprecision at the boundaries between regions, which correspond to a lack of knowledge, is accounted for in the modelling. Moreover, considering the large amount of noise, our method outperforms a simple FCM [10], the method proposed in [21], and also the ECM algorithm [11] and its extension proposed in [20].

Our method is generic because it can be applied regardless of what the distribution of initial beliefs is. In future work, we plan to test our method on a larger database to assess the robustness of the method and on other types of images to confirm its genericity.

## References

[1] A. Dempster, Upper and lower probabilities induced by a multivalued mapping, Ann. Math. Stat. 38 (1967) 325–339.
[2] G. Shafer, A Mathematical Theory of Evidence, Princeton University Press, 1976.
[3] P. Smets, R. Kennes, The transferable belief model, Artif. Intell. 66 (1994) 191–234.
[4] A. Appriou, Formulation et traitement de l'incertain en analyse multi-senseur, in: 14ème Colloq. GRETSI, Juan-les-Pins, 1993, pp. 951–954.
[5] P. Smets, Belief functions: The disjunctive rule of combination and the generalized Bayesian theorem, Int. J. Approx. Reason. 9 (1993) 1–35.
[6] I. Bloch, Some aspects of Dempster–Shafer evidence theory for classification of multi-modality medical images taking partial volume effect into account, Pattern Recognit. Lett. 17 (1996) 905–919.
[7] N. Milisavljevic, I. Bloch, Sensor fusion in anti-personnel mine detection using a two-level belief function model, IEEE Trans. Syst. Man Cybern. 33 (2003) 269–283.
[8] T. Denœux, A $k$-nearest neighbor classification rule based on Dempster–Shafer theory, IEEE Trans. Syst. Man Cybern. 25 (1995) 804–813.
[9] A.S. Capelle-Laize, O. Colot, C. Femandez-Maloigne, Evidential segmentation scheme of multi-echo MR images for the detection of brain tumors using neighborhood information, Inf. Fusion 5 (2004) 203–216.
[10] J.C. Bezdek, Pattern Recognition with Fuzzy Objective Function Algorithms, Kluwer Acad. Publ., Norwell, MA, USA, 1981.
[11] M.-H. Masson, T. Denœux, ECM: An evidential version of the fuzzy c-means algorithm, Pattern Recognit. 341 (2008) 1384–1397.
[12] V. Antoine, B. Quost, M.-H. Masson, T. Denoeux, CECM: Constrained evidential C-means algorithm, Comput. Stat. Data Anal. 56 (2012) 894–914.
[13] M.-H. Masson, T. Denœux, RECM: Relational evidential c-means algorithm, Pattern Recognit. Lett. 30 (2009) 1015–1026.
[14] T. Denœux, M.H. Masson, EVCLUS: evidential clustering of proximity data, IEEE Trans. Syst. Man Cybern. 34 (2004) 95–109.
[15] M. Rombaut, Y.M. Zhu, Study of Dempster–Shafer theory for image segmentation applications, Image Vis. Comput. 20 (2002) 15–23.
[16] W. Pieczynski, D. Benboudjema, Multisensor triplet Markov fields and theory of evidence, Image Vis. Comput. 24 (2006) 61–69.
[17] S.L. Hégarat-Mascle, I. Bloch, D. Vidal-Madjar, Introduction of neighborhood information in evidence theory and application to data fusion of radar and optical images with partial cloud cover, Pattern Recognit. 31 (1998) 1811–1823.

[18] P. Vannoorenberghe, E. Lefevre, O. Colot, Traitement d'images et théorie des fonctions de croyance, in: Actes des XII$^{èmes}$ Rencontres Francophones sur la Logique Floue et ses Applications, 2003, pp. 287–294.
[19] P. Zhang, I. Gardin, P. Vannoorenberghe, Information fusion using evidence theory for segmentation of medical images, in: Int. Colloq. Inf. Fusion, vol. 1, 2007, pp. 265–272.
[20] N. Makni, N. Betrouni, O. Colot, Introducing spatial neighbourhood in evidential C-means for segmentation of multi-source images: application to prostate multi-parametric MRI, Int. J. Inf. Fusion (2012) 1–12, in press.
[21] I. Bloch, Defining belief functions using mathematical morphology – Application to image fusion under imprecision, Int. J. Approx. Reason. 48 (2008) 437–465.
[22] B. Lelandais, I. Gardin, L. Mouchard, P. Vera, S. Ruan, Using belief function theory to deal with uncertainties and imprecisions in image processing, in: 2nd Int. Conf. Belief Function, 2012, pp. 197–204.
[23] Z. Elouedi, E. Lefevre, D. Mercier, Discountings of a belief function using a confusion matrix, in: Int. Conf. Tool. Artif. Intell., 2010, pp. 287–294.
[24] M.K. Gould, W.G. Kuschner, C.E. Rydzak, C.C. Maclean, A.N. Demas, H. Shigemitsu, J.K. Chan, D.K. Owens, Test performance of positron emission tomography and computed tomography for mediastinal staging in patients with non-small-cell lung cancer: a meta-analysis, Ann. Intern. Med. 139 (2003) 879–892.
[25] B. Xu, Z. Guan, C. Liu, R. Wang, D. Yin, J. Zhang, Y. Chen, S. Yao, M. Shao, H. Wang, J. Tian, Can multimodality imaging using 18F-FDG/18F-FLT PET/CT benefit the diagnosis and management of patients with pulmonary lesions?, Eur. J. Nucl. Med. Mol. Imaging 38 (2011) 285–292.
[26] W. Choi, S.W. Lee, S.H. Park, J.S. Ryu, S.J. Oh, K.C. Im, E.K. Choi, J.H. Kim, S.H. Jung, S. Kim, S.D. Ahn, Planning study for available dose of hypoxic tumor volume using fluorine-18-labeled fluoromisonidazole positron emission tomography for treatment of the head and neck cancer, Radiother. Oncol. 97 (2010) 176–182.